Peer Reviewed Paper openaccess

A semi-supervised cycle-GAN neural network for hyperspectral image classification with minimum noise fraction

Tatireddy Subba Reddy[a,b] and Jonnadula Harikiran[c,*]

[a]Research Scholar, School of Computer Science and Engineering, VIT-AP University, Amaravathi, Andhra Pradesh-522237, India

[b]Assistant Professor, Department of Computer Science and Engineering, B V Raju Institute of Technology, Narsapur, Medak, Telangana, India

[c]Associate Professor, School of Computer Science and Engineering, VIT-AP University, Amaravthi, Andhra Pradesh-522237, India

Contact
Tatireddy Subba Reddy: tatireddysubba12@gmail.com
https://orcid.org/0000-0002-6534-5400
Jonnadula Harikiran: jonnadulaharikiran@gmail.com

Hyperspectral imaging (HSI) is a popular mode of remote sensing imaging that collects data beyond the visible spectrum. Many classification techniques have been developed in recent years, since classification is the most crucial task in hyperspectral image processing. Furthermore, extracting features from hyperspectral images is challenging in many scenarios. The semi-supervised classification of HSI is motivated by the Cycle-GAN method that has been proposed in this research paper. Since the proposed HSI classification method is semi-supervised, it makes extensive use of the labelled samples, which are short and have numerous unlabelled images. The research is carried out in two phases. First, to extract the spectral–spatial features, the minimum noise fraction is adopted. And, second, the classification of the semi-supervised method is done by the cycle-GANs. Subsequently, the proposed architecture is implemented on three standard hyperspectral dataset methods. As a result, the performance comparison is carried out in the same field as state-of-the-art approaches. The obtained results successfully demonstrate the supremacy of the proposed technique in the classification of HSI.

Keywords: feature extraction, hyperspectral image, cycle-GANs, semi-supervised classification, minimum noise fraction (MNF), AVIRIS sensors, rolling guidance filter (RGF), Indian Pines, transductive support vector machine (TSVM), convolutional neural networks (CNN)

Introduction

Hyperspectral imaging (HSI) research is now widely used in various fields, including land coverage classification, monitoring and quality control, environmental science and industrial applications.[1,2] It has been much used in the fields of security, urban planning and mining technology. Hyperspectral images are 3D data cubes, that contain 1D-spectral information (spectral bands) and 2D-spatial information (image feature).[3,4] The spectral bands contain fine wavelengths, while dispersion and correlation are visible among nearby pixels from various angles on images of confident wavelength characteristics, like shape and land cover.[5,6] There are numerous

Correspondence
Jonnadula Harikiran (jonnadulaharikiran@gmail.com)

Received: 15 October 2021
Revised: 15 December 2021
Accepted: 31 January 2022
Publication: 29 March 2022
doi: 10.1255/jsi.2022.a2
ISSN: 2040-4565

Citation
T.S. Reddy and J. Harikiran, "A semi-supervised cycle-GAN neural network for hyperspectral image classification with minimum noise fraction", *J. Spectral Imaging* **11,** a2 (2022). https://doi.org/10.1255/jsi.2022.a2

issues with HSI processing, including high dimensionality, computational complexity, poor contrast, noise and a lack of training samples. To overcome the dimensionality issue, techniques of pre-processing such as minimum noise fraction (MNF),[7–9] randomised principal component analysis (R-PCA) etc. are employed to extract the most appropriate features. The large number of spectral bands, which produce a dimensionality of high degree data, poses a challenge to image analysis and classification.[10,11] Various types of classifiers have been developed over the last few decades to solve the above-mentioned problems. They can be organised into three main categories, i.e. semi-supervised methods, unsupervised methods and supervised methods.[12,13] In unsupervised methods, large unlabelled samples are used to train the models. Because unsupervised methods can easily handle hyperspectral data, no labelled samples are required. Several unsupervised methods, such as C-means, graph-based, artificial immune algorithm, fuzzy clustering, fuzzy and others have outperformed the supervised methods in hyperspectral classification. It is impossible to determine the relationship between clusters and classes due to a lack of prior knowledge.[14,15]

The semi-supervised techniques of learning try to solve the "small sample problem" by combining the advantages of both a limited number of labelled data with a large number of unlabelled samples that are easily available. Semi-supervised methods are organised into four categories: (1) the generative models, by which the densities of the condition to get the sample labels are evaluated.[16,17] (2) Separation of low-density, in which the boundaries are placed in the areas where some samples are obtainable (labelled or unlabelled). The transductive support vector machine (TSVM) is the chief among the state-of-the-art algorithms. (3) Labelled and unlabelled samples that are utilised by graph-based methods and assign labels to unlabelled samples. (4) Wrapper-based methods, in which in every iteration of the method of supervised learning, the unlabelled samples are labelled gradually. Self-training and co-training are the most frequently used wrapper-based methods.

Unfortunately, the methods mentioned above can only extract a few features from the HSI dataset. Deep learning has emerged as a hotspot in image processing, particularly in hyperspectral classification, according to recent research. Deep brief networks (DBN), convolutional neural networks (CNN) and stacked autoencoders (SAE) are common deep architectures.[18] For training to carry out frameworks of supervised classification, a large number of labels must be granted. Using a semi-supervised classifier following contextual deep learning and multi-decision labelling (CDL-MD-L), the current work has demonstrated hopeful results in the classification of the hyperspectrum.[19,20]

A significant number of labelled samples are required for training the frameworks of supervised classification. However, the semi-supervised approach can handle both labelled and unlabelled samples. Semi-supervised learning takes over by increasing the generator samples for feature extraction and maximising the output of the classifier dimension. Here, the proposed semi-supervised framework drives to promising results, outperforming some existing methods.

The main contributions of this research include:

- A new framework for semi-supervised spectral–spatial HSI classification is introduced.
- The noise in the HSI may be reduced more effectively by incorporating the MNF during dimensionality reduction.
- To improve the accuracy of classification, the proposed cycle-generative adversarial networks (cycle-GANs) technique for the classification of HSI uses spatio–spectral features.
- The proposed technique is estimated on three broadly utilised HSI datasets and hopeful results are found.

Literature review

Recently, many researchers have focused on improving classification accuracy via semi-supervised learning frameworks.

A semi-supervised classification algorithm combining the methods of deep learning and clustering for HSI was introduced by Wu *et al.*[21] They addressed the problem of excessively unlabelled samples happening in hyperspectral images that are solved by a self-training algorithm, in which the labelled samples are expensive. First, by using CNN the spatial–spectrum features were extracted. Then for clustering of semantic constraint, the extracted spectral–spatial features were utilised. Once the results of clustering for all the images had been received, using local decisions the pseudo labels were flattened. They compared the algorithm to spatial neighborhood information (SNI)-unit, SNI-L and contextual deep learner (CDL), respectively. On comparing the other three algorithms, the overall accuracy (OA), average accuracy (AA) and Kappa of the proposed algorithm was higher. Cui *et al.*[22] presented a classification of the semi-supervised method with regards to Rolling guidance filter (RGF) and

extended label propagation (ELP) said to be RGF-ELP. ELP is a fresh two-step process that makes use of all the unlabelled samples. They broadcast the information of the label from labelled to unlabelled samples around in the starting step by using graph-based label propagation. From the segmentation of the image, the next step was to allocate similar labels to every pixel through the superpixels generated, modifying any labels that were improperly labelled over the last step. In addition, to enhance the initial hyperspectral image, the RGF was used to eliminate the noise and small textures which is an effective method of feature extraction. At last, to train a support vector machine (SVM) these introductory labelled and high-confidence pseudo located samples were utilised.

A super pixel-level method of classification, depending on the graph and discrete potential (SSC-GDP) for HSI was suggested by Zhao *et al.*[23] To produce a connectivity weighted graph and to split the weighted graph is the key concept of this method. Using the weighted connection between the superpixel and its spatial neighbourhood depending on the segmentation of the superpixel is constructed by the weighted connectivity graph. Then, the created graph was divided into various sub-graphs using an improved algorithm of semi-supervised Wu–Huberman (ISWH). Two benchmarks which are publicly available, such as the Salinas and Indian Pines, were used for the performance testing approach for proving the spectral–spatial method effectiveness of the proposed.

Boggavarapu and Manoharan[24] analysed the spatio–spectral features and uncorrelated bands extraction and texture patterns exploitation via analysis of the Gabor filter and exploratory factor, respectively. Then, in each of the factor analysis variables, they enclosed these features to the real cube basically the noise is heteroscedastic. To classify the hyperspectral cube labels, three-dimensional CNNs are used. Experiments are carried out on the datasets of three benchmarks such as Salinas, University of Pavia and Indian Pines.

Based on a superpixel pooling CNN (SP-CNN) with transfer learning classification of spectral–spatial HSI technique was developed by Xie *et al.*[25] This method comprises three stages. Convolution and pooling in the first stage, and through downsampling, it extracts the major spectral HSI characteristics. They combined up-sampling with the pooling of superpixels in the second part. Finally, the hyperspectral data is nourished to CNN as a pixel. The information of the spectral and spatial is efficiently combined by the technique of superpixel pooling usage in this method.

For performance improvement, the reduction of auto-encoder-based dimensionality was suggested by Ramamurthy *et al.*[26] To enhance the accuracy, the pixel has been constructed again using vectors and the loss of reconstruction was found. The classification process for hyperspectral images was applied by the CNN framework. The presented technique was related to the other existing techniques of SVM, spectral–spatial residual network (SSRN) for different parameters.

For hyperspectral image classification, the hybrid CNN model based on the multiple scale spatio–spectral features is developed by Mohan and Venkatesan.[27] A linear Gaussian random projection (GRP) and non-linear kernel principal component analysis (KPCA) were handled by a hybrid technique, which was used for the extraction of the optimal band. For varying sizes of the window using 3D-CNN, the hybrid classification of the CNN technique extracts the features of spatial and spectral methods. For the additional feature extraction and classification, the features were linked and carried into a 2D-CNN. Against several state-of-the-art methods, the CNN-based techniques were related to the hybrid model.

Problem statement

One of the key concepts of a hyperspectral image is the presence of a large number of small, adjacent spectral bands containing various information. This information can be utilised in the applications of remote sensing like classification of land cover, analysis and crop protection, and detection of minerals. In most applications, pixel classifications in a hyperspectral image are crucial. Although there are several challenges affiliated with this task, the most prominent barrier is the lack of perfectly labelled pixels. Moreover, compared to the dimensions of the spectrum of the hyperspectral image, the absence of labelled pixels results in a comparatively small amount of training data. This introduces the dimensionality curse to this application. Hyperspectral images have numerous spectral dimensions, some of which are surplus. Thus, extracting distinct features plays a crucial role in the process of classification by decreasing the input data dimensionality. To accomplish this, we present effective techniques for reducing dimensionality and HSI pixel classification.

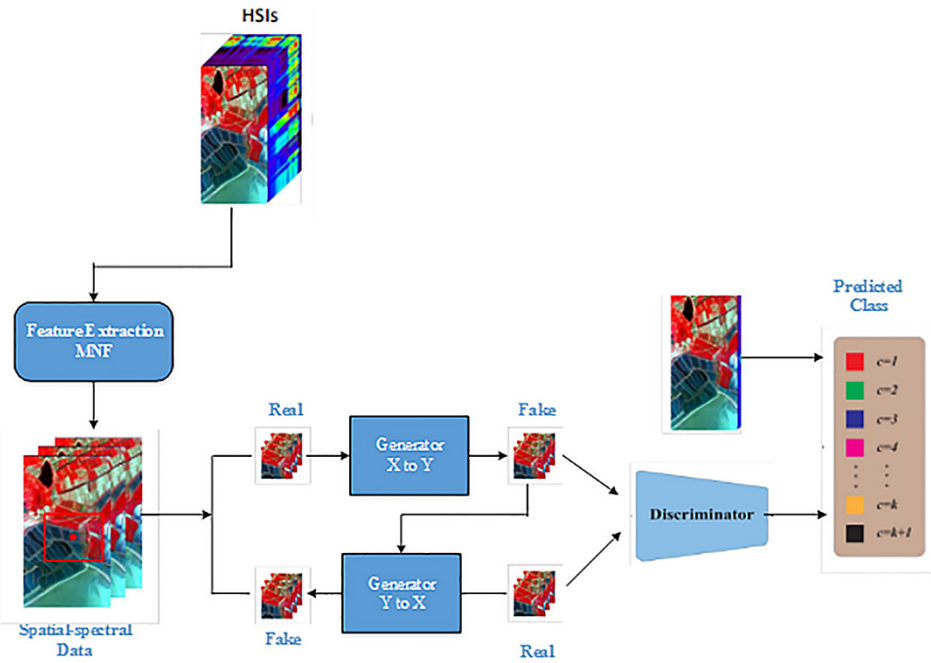

Figure 1. Proposed methodology.

Methodology

The dual parts of the proposed methods' conceptual architecture are shown in Figure 1. The spatial and spectral features are extracted in the first part using MNF. As a result, the cycle-GANs are used for the classification feature space of the method of semi-supervision, taking full advantage of both limited labelled and enough unlabelled samples. The classification map is a visual representation of accuracy results for different samples.

Feature extraction

Feature extraction is the extraction of relevant information from an information class. Since features are the necessary elements of any data set, feature extraction is essential in the learning process. The extraction of features for HSI classification can be divided into two phases, such as (i) spatial feature extraction and (ii) spectral feature extraction. This can be done by adopting the MNF transform.

The MNF transform is used to remove correlations between bands or to reduce data noise. By taking the original matrix $\mathbf{X} \in \mathbf{R}^{M \times N}$ spectral data and the matrix of transformation $\mathbf{W} \in \mathbf{R}^{d * M}$, the HSI bands number are denoted as *N*, *M*, where, *N*, *M* is the HSI pixel number, also the data's size of a new dimension is denoted as *d*. The features extraction matrix of MNF $\mathbf{Y} \in \mathbf{R}d \times N$ can be mathematically represented and given as:

$$\mathbf{Y} = \mathbf{W}^{\mathrm{T}}\mathbf{X} \tag{1}$$

Here, the original data matrix is "**X**", **S** is the signal part and **N** is the additive noise part and represented as shown in (2):

$$\mathbf{X} = \mathbf{S} + \mathbf{N} \tag{2}$$

Consequently, the matrix of covariance "**X**" is equal to the sum of the matrices of noise and signal and denoted as below:

$$\sum_{\mathbf{X}} = \sum_{\mathbf{S}} + \sum_{\mathbf{N}} \tag{3}$$

where $\sum_{\mathbf{N}}$ is the covariance of noise and $\sum_{\mathbf{S}}$ is the covariance of the signal. The MNF's goals are to create new features (**Y**) that can be classified by their signal-to-noise ratio, as a linear transformation. It is given as follows by calculation:

$$\arg\max_{\mathbf{W}} \frac{\mathbf{W}^{\mathrm{T}} \sum x \mathbf{W}}{\mathbf{W}^{\mathrm{T}} \sum \mathbf{N}\mathbf{W}} - 1 \tag{4}$$

W should be made up of the eigenvectors connected with classified eigenvalues of $\sum_{\mathbf{X}}$. MAF (factor of minimum/maximum auto-correlation) is used to calculate the covariance of noise $\sum_{\mathbf{N}}$ in this research paper. Two stages are involved in this method. First, noisy images are generated from every band of HSI as shown in formula (5):

$$\text{Noise image} = x_{(i,j,k)} - x_{(i+\Delta 1, j+\Delta 2, k)} \tag{5}$$

As shown in (5), k denotes the k^{th} spectral band of the image of HSI in "i" and "j". i and j represent the pixels rows and columns. Spatial lags Δ1 and Δ2 along each axis of coordinate are generally assumed to be 1. According to (6), we calculate the noise covariance Σ_N.

$$\Sigma_N = 0.5 \text{ (Noise image)} \tag{6}$$

Filters can be applied to the bandwidth that has the least noise level; this effectively removes noise from the data. Then, the data is transmitted back to its original coordinate system. MNF is said to be a linear transformation.

Classification

Traditionally, the accuracy of a classifier is determined by the number of training samples. As an outcome, increasing the number of labelled training samples improves the classifier's performance. Although retrieving and labelling samples on this site is difficult. In hyperspectral imaging, spectral samples are made up of a combination of pure and impure signatures, with impure signatures containing more samples (HSI). As a result, the training data are mislabelled in the samples of the mixed signatures. It is simple to create new training samples with semi-supervised learning (SSL) by combining a few previously labelled training samples. SSL techniques do not solve the mislabelling problem, but they can help to increase the number of samples that are correctly labelled. In this way, mislabelled sample rates in training data could be reduced. Cycle-GAN is employed to classify the extracted features. In cycle-GAN, two GANs are duplicated and form a ring. The transformation of class A in another domain to generate class A1 is a key component of cycle-GAN and then again converting A1 back to A, in which A1 represents a matching between the input class A and the output image "A1". Without pairing, cycle-GAN has the advantage of training the pair of two classes.

Cycle-GAN for semi-supervised learning

A supervised learning task normally performs an unsupervised learning task. There are a few cases where there are not enough training samples. Furthermore, incorporating new training samples may be difficult. SSL, as previously said, is a learning method that can learn with a minimal amount of training data, bridging the gap between unsupervised and supervised learning. A sample generation of N classes illustrates how SSL can be applied to GAN. The discriminator is extended to $N+1$ outputs, including information about their classification and a term that signifies their origin. The GAN sample generation is more transparent than the conventional GAN. In this proposed method, SSL is applied to cycle-GAN, which implies both trained labelled samples and trained unlabelled samples.

Cycle-GAN is a mapping model for domains **X** and **Y**. Two GANs are used in cycle-GAN: two generators and two discriminators. Generators consist of G_{XtoY} and G_{YtoX} as mapping to each domain. Discriminators consist of D_X and D_Y as identification of each domain. For $\mathbf{X} \rightarrow \mathbf{Y}$ mapping, the purpose of G_{XtoY} is to let D_Y identify that the translation data $G_{XtoY(x)}$ was sampled from domain **Y**. G_{XtoY} is meant to determine whether the input sample came from the domain **Y** or was translated by D_Y. In the same way, mapping **Y** to **X** is accurate. Samples are created by generators based on desired distributions, i.e. replicating the expected distribution. The discriminator is used to distinguish real samples from those generated by the generator. The networks (generator and discriminator) are trained at the same time until the generator generates samples that are so realistic that the discriminator cannot make a distinction between real and fake samples. This stage is called equilibrium. When the model reaches this equilibrium stage, it automatically stops training. The input sample is passed to the encoder in the first step. It is compressed to represent each sample using convolutions, and a sample feature is extracted from the input image. The representation by 1/4 of the actual sample size is decreased by the encoder that has three convolutions. An input sample of sizes 27, 27, 3 will result in an encoder output of 3, 3 and 27. In the transformer section, the encoder output will be activated after the activation function has been applied. Transformers generally contain 6/9 residual blocks based on their input size. The outputs of transformers are used as decoder inputs. Two blocks of fraction stride deconvolution are used to increase the size of the representation.

Loss functions

Cycle-GAN has two loss functions: adversarial loss (L_{adv}) and cycle consistency loss (L_{cyc}). The loss function is minimised by generators. Loss functions are maximised by discriminators.

$$\begin{aligned} &L(G_{XtoY}, G_{YtoX}, D_X, D_Y) = \\ &L_{adv}(G_{XtoY}, G_{YtoX}, D_X, D_Y) + \lambda L_{cyc}(G_{XtoY}, G_{YtoX}) \end{aligned} \tag{7}$$

taking λ as the weight for L_{cyc}. The loss functions are described as follows.

GAN uses adversarial loss as a loss function. Distance between probability distributions is expressed here. There are two terms, one mapping from domain **X** to domain **Y**, and one mapping from domain **Y** to domain **X**.

$$L_{GAN}(G,D_Y,\mathbf{X},\mathbf{Y}) = \\ \mathring{A}_y \sim_{pdata}(y)[\log D_Y(y)] + E_x \sim_{pdata}(x)[\log 1 - D_Y(G(x))] \quad (8)$$

where $\hat{x}$ and $\hat{y}$ are pair data of y and x, respectively. That is, $\hat{x} = \hat{y}, \hat{x} = \hat{y}, \hat{x} = y = \hat{x}$. Learning with non-pair data is done with the conventional loss function. The proposed method results in the following loss function,

$$L(G_{XtoY},G_{YtoX},D_X,D_y) \\ = \begin{cases} kL_{sv}(G_{XtoY},G_{YtoX}), & \text{real sample} \\ L_{adv}(G_{XtoY},D_Y) + L_{adv}(G_{YtoX},D_X) & \\ +\lambda L_{cyc}(G_{XtoY},G_{YtoX}), & \text{otherwise} \end{cases} \quad (9)$$

where κ is the weight of L_{adv}.

Experimental results and discussion

The purpose of this section is to assess the performance of the proposed method on the three benchmark HSI datasets. We carried out experiments to compare the proposed method to other existing methods such as 3D-CNN, SVM, 2D-CNN and spectral–spatial unified networks (SSUN). Then, the efficacy of the proposed technique is evaluated for various parameters.

Experimental dataset description

The efficiency of the designed model in this research is evaluated using existing approaches employing the three hyperspectral datasets. They are Salinas Scene (SS), Pavia University (PU) and Indian Pines (IP) (http://www.ehu.eus/ccwintco/index.php?title=Hyperspectral_Remote_Sensing_Scenes).

In this dataset, AVIRIS sensors are used to collect data from the IP test site. The spectral images of IP are 145 × 145 pixels in size. Between 0.4 m and 2.5 m, the sensor recorded 224 spectral bands. Some of the 224 bands have complete water absorption. After removing the water-absorbing bands, 200 bands are used in the experiments. A total of 16 class labels have been identified in the IP dataset. The PU images are collected using ROSIS-03 optical sensors in the wavelength range of 0.43–0.86 µm. This HSI dataset consists of 104 spectral images with a size of 610 × 340 pixels and a geometry resolution of 1.3 m. The image of the ground truth is divided into nine classes. The AVIRIS sensor was used to capture the SS dataset in the Salinas Valley area of California. The water absorption area of 20 bands from the IP dataset was detached, thus only 204 of the original 224 bands were used in this experiment. Each spectral data consist of a 3.7 m resolution and a spatial resolution of 512 × 214 pixels with ground truth labels of 16 classes.

Experimental setup

Deep learning methods are heavily parameterised and so many training samples are needed to ensure accuracy. For all the experiments, the values for κ and λ are based on the average performance of the held-out validation set in HSI. For training the cycle-GAN network, the parameter of the network is initialised and is listed in Table 1. With a batch size of 1, the models were trained, 200 epochs for training and Adam optimisation is used to tune the parameters with a learning rate of 0.0001.

Then, the hyperspectral images were used for pixel-by-pixel classification, because ground truth data were-captured within the field of observation. In this research, Python is used for implementation. The proposed technique is related to the existing SVM, 3D-CNN, 2D-CNN and spectral–spatial unified network (SSUN) techniques for various parameters. A train or test sample is one pixel, which is $1 \times b$ in size in this experiment. Each pixel is carried as a specific class feature and classified by the cycle-GANs discriminator or various classifiers. Every pixel specifies a distinct label. The entire cube is composed of many pixels and labels. All HSI datasets are structured between 0 and 1 at the beginning of the experiments. Every experiment is carried out on the normalised hyperspectral datasets, and the data available is divided into two categories: 60% for sample training and 40% for sample testing. Only a few labelled images are used in each dataset, with five samples for each class randomly selected from the training samples as labelled samples and the rest used as unlabelled samples. The AA is declared and the experiments are repeated ten times using random selection on the sets of training and testing. The methods used to estimate the results of

Table 1. Parameter initialisation of cycle-GAN.

Index	Parameters	Value
1	Image size	145 × 145
2	Batch	1
3	Learning rate	1×10^{-4}
4	Pool size	50
5	λ	27
6	κ	10

quantitative experiments by three popular indices, OA, AA and κ, are compared.

Evaluation parameters

The parameters Kappa statistics (κ), AA and OA were utilised to compare the proposed methodology classification to existing state-of-the-art methods.

The OA is calculated by dividing the proportion of accurately identified samples by the total number of test samples. It is a $C \times C$ square matrix, where C denotes the dataset's collection of class labels. The formula for computing OA from a confusion matrix is as follows:

$$OA = \sum_{i=1}^{C} \frac{t_{ii}}{t} \tag{10}$$

The set of successfully identified for class samples i is denoted by t_{ij}, while the total test samples are denoted by t. The diagonal-wise elements of the confusion matrix are used to calculate t_{ij}.

Average accuracy: the mean of class-wise accuracy is denoted by AA, and the confusion matrix is used to determine the accuracy of each class:

$$CA_i = \frac{t_{ii}}{\sum_{j=1}^{C} t_{ij}} \tag{11}$$

In class i, CA_i stands for class-wise accuracy and the number of class i samples categorised into class j is denoted by t_{ij}, i.e. CA is the difference between the total set of test samples in the same class and the fraction of correctly classified samples for class i. The definition of AA is

$$AA = \frac{\sum_{i=1}^{C} CA_i}{C} \tag{12}$$

The row and column total of the confusion matrix represents the likelihood of agreement between the classified and actual results. The difference between these two numbers is the Kappa statistic. The κ value ranges from −1 to 1, and as κ approaches 1, the accuracy of the classification increases. The sum of the row elements

$$\left(\sum_{j=1}^{C} t_{ij}\right)$$

is t_{i+} and in the confusion matrix for class i, t_{+i} is the addition of column elements in column-wise

$$\sum_{i=1}^{C} t_{ij} .$$

The value of the κ is determined as

$$\mathrm{K} = \frac{t\sum_{i=1}^{C} t_{ii} - \sum_{i=1}^{C} t_{i+}t_{+i}}{n^2 - \sum_{i=1}^{C} t_{i+}t_{+i}} \tag{13}$$

Result analysis

The hyperspectral data are improved by applying the feature extraction technique to each dataset based on the classification of dissimilar objects. The output of the spectral band is used in the proposed classification procedure, which is based on the concept of an adversarial network. The accuracy of the classification stage is improved by implementing a feature extraction technique. The SVM is the most well-known multiclass classification algorithm. Despite its limited sensitivity, SVM has a high classification accuracy. For comparing the results, SVM on a radial basis was chosen. Then, for performance evaluation, we choose a 2D-CNN. PCA is chosen as a method of pre-processing by a 2D-CNN model, which also chooses the first principal component. Because the models of 2D-CNN extract only local spatial features, 3D-CNN chose a diverse existing model to compare with the spatial–spectral technique of feature extraction. It performs three-dimensional convolution and thus the model of 3D-CNN chooses a neighbourhood of $K \times K \times B$ for each pixel. Finally, we chose SSUN as one of the existing models to compare results.

Comparative study

In this section, the proposed method (cycle-GAN) is compared to other DL-based methods, such as 2D-CNN,

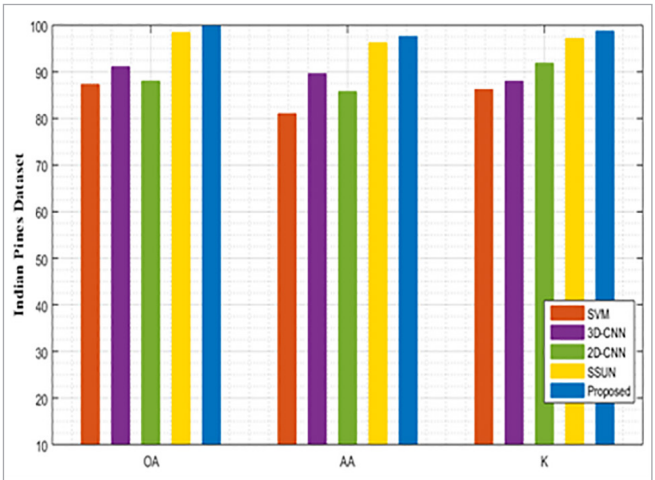

Figure 2. Comparison results classification on the IP dataset.

Table 2. Evaluation parameters classification for the IP datasets using various methods.

Methods	Indian Pines dataset		
	OA	AA	κ
SVM	87.3	81.03	86.2
3D-CNN	91.1	89.58	87.98
2D-CNN	87.99	85.75	91.85
SSUN	98.4	96.23	97.14
Proposed method cycle-GAN	99.80	97.56	98.72

3D-CNN, SVM and SSUN. Figures 2, 4 and 6 show the classification results for Kappa coefficient, AA and OA on the SS, PU and IP datasets, respectively. The results of the experiments show that the proposed method extracts spatial–spectrum features effectively and has better classification accuracy for hyperspectral images.

On the IP dataset, Table 2 displays the obtained κ, AA and OA for SVM, 3D-CNN, 2D-CNN and SSUN, as well as the proposed cycle-GAN technique. The lower rates κ, AA and OA are greater than the other methods and the accuracy values of the cycle-GAN classification approach are noticeable based on the obtained results. The accuracy of OA is 99.80% for cycle-GAN, and it is 98.4% for SSUN, 87.99% for 2D-CNN, 87.99% for 3D-CNN and 87.93% for SVM. The obtained OA of the cycle-GAN method is nearer to the OA of SSUN. SVM has the lower rates with an OA of 87.93%. Figure 3 illustrates the classification map and ground truth of the IP dataset. The classification map for the proposed approach and the ground truth are similar, i.e. the amount of misclassification is minimum.

Table 3 exhibits the accuracy rates for PU. In addition, when compared to SVM, 3D-CNN, 2D-CNN, SSUN and Cycle-GAN, the proposed cycle-GAN outperforms them all, with an OA of 99.54%. The least classification rates are acquired with the 2D-CNN method, which has an accuracy of OA of 87.99%. The PU dataset map classification is shown in Figure 3.

Figure 6 demonstrates the classification map for the SS dataset. Table 4 shows the classification results for the SS dataset. In addition, it can be seen that the proposed approach is more efficient than other existing methods in every case of OA, AA and κ. The OA of the proposed

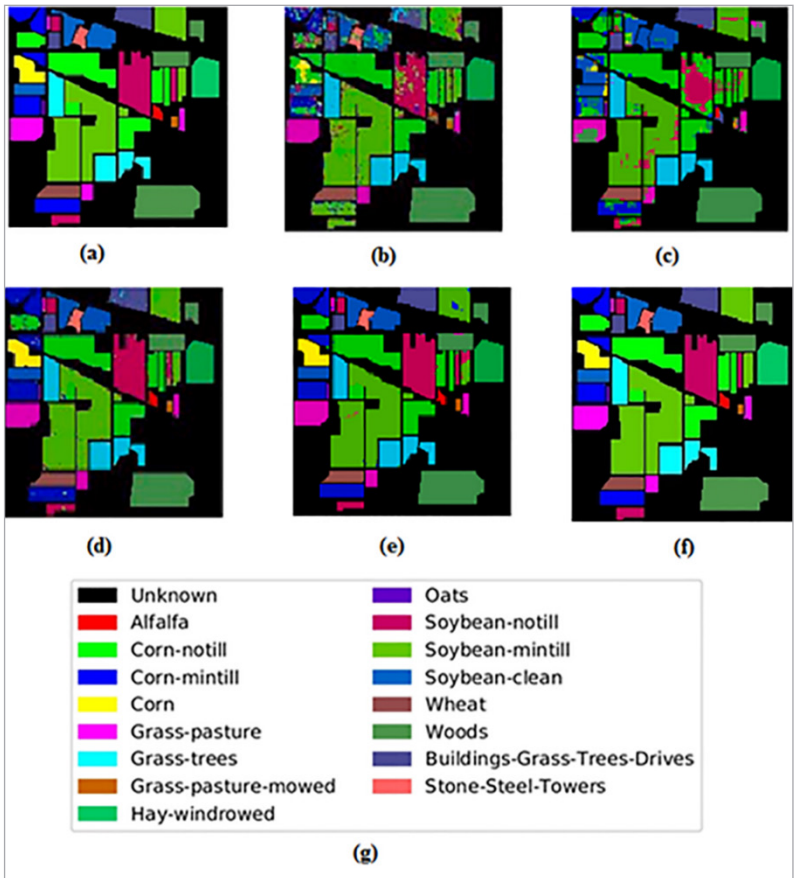

Figure 3. IP dataset classification map of (a) ground truth, (b) 2D-CNN, (c) SVM, (d) SSUN, (e) 3D-CNN, (f) proposed and (g) legend.

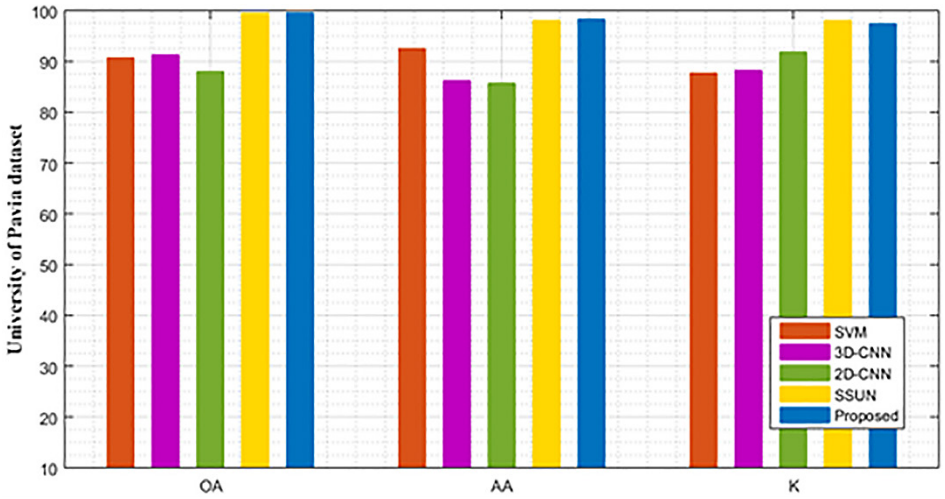

Figure 4. Classification comparison results on PU dataset.

Table 3. Classification of parameters evaluation for the PU datasets using different methods.

Methods	University of Pavia dataset		
	OA	AA	κ
SVM	90.71	92.55	87.71
3D-CNN	91.3	86.19	88.21
2D-CNN	87.99	85.75	91.85
SSUN	99.46	98.03	98.04
Proposed method Cycle-GAN	99.54	98.32	97.42

Table 4. Evaluation parameters classification for the SS datasets using various methods.

Methods	Salinas Scene dataset		
	OA	AA	κ
SVM	90	95.52	88.82
3D-CNN	93.59	96.99	94.26
2D-CNN	87.99	85.75	91.85
SSUN	98.82	98.21	97.75
Proposed method Cycle-GAN	98.57	99.88	99.57

approach is 98.57%, AA is 99.88% and κ is of 99.57%. The obtained OA with Cycle-GAN is 98.57%, which is nearer to SSUN.

Another parameter used for the comparision of proposed technique to the existing method is execution time. Deep learning models are designed to reduce computational complexity. The proposed technique reduces computations, thereby reducing the training time for classification and feature extraction.

Table 5 illustrates the time of training and time of testing for existing and proposed techniques on the datasets of SA, IP and PU. And, the time of training is measured in terms of minutes, the time of testing by seconds here.

Figures 8–10 represents the testing and training time for the proposed technique in comparison to the existing methods despite computing the hyperspectral image classification from the dataset.

Analysis of parameters in cycle-GAN

λ and κ are the parameters of cycle-GAN. The input size of spatial patches is denoted by λ, which is set to current approaches. The updated intervals of G1 and G2 generators in relation to discriminator D are represented by κ. It is set to the existing technique. κ controls the balance between generators and discriminators. Cycle-GAN does not extract enough information regarding the spatial distribution of HSI, when λ is too small. In contrast, if λ is too large, Cycle-GAN is unable to represent the samples accurately. Finally, 27 is selected for λ among the three hyperspectral data sets and κ is equal to 10 or 13. Here, κ is selected as 13, so that the OA of the three data sets achieves the highest peak values. Hence, the experiment revealed that, by adjusting the weight to suitable

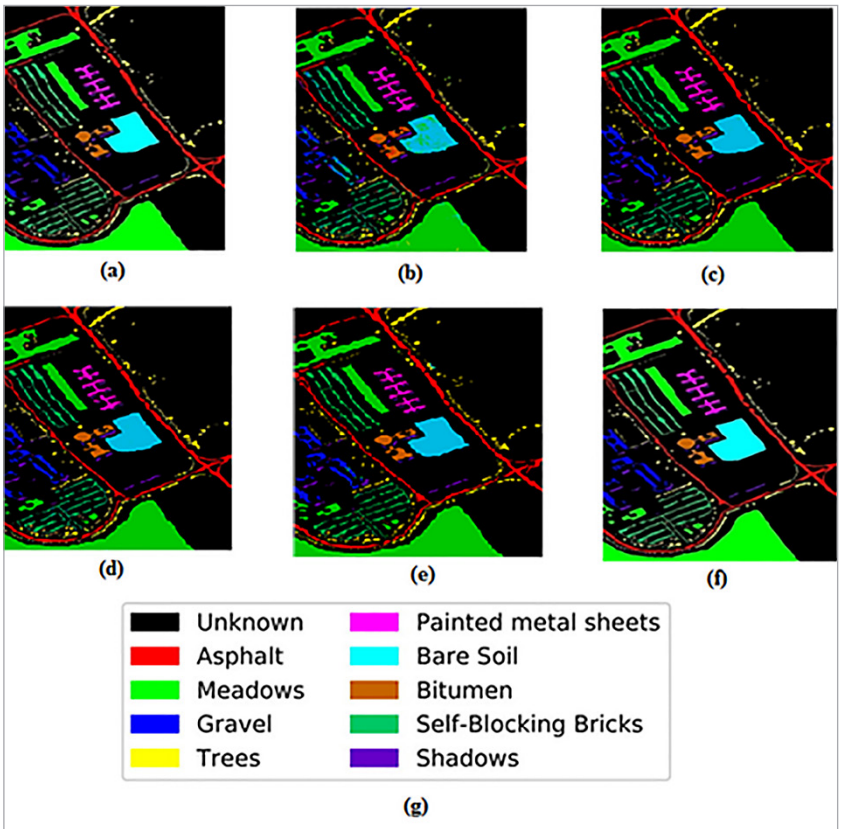

Figure 5. PU dataset classification map. (a) Ground truth, (b) 2D-CNN, (c) SVM, (d) SSUN, (e) 3D-CNN, (f) proposed and (g) legend.

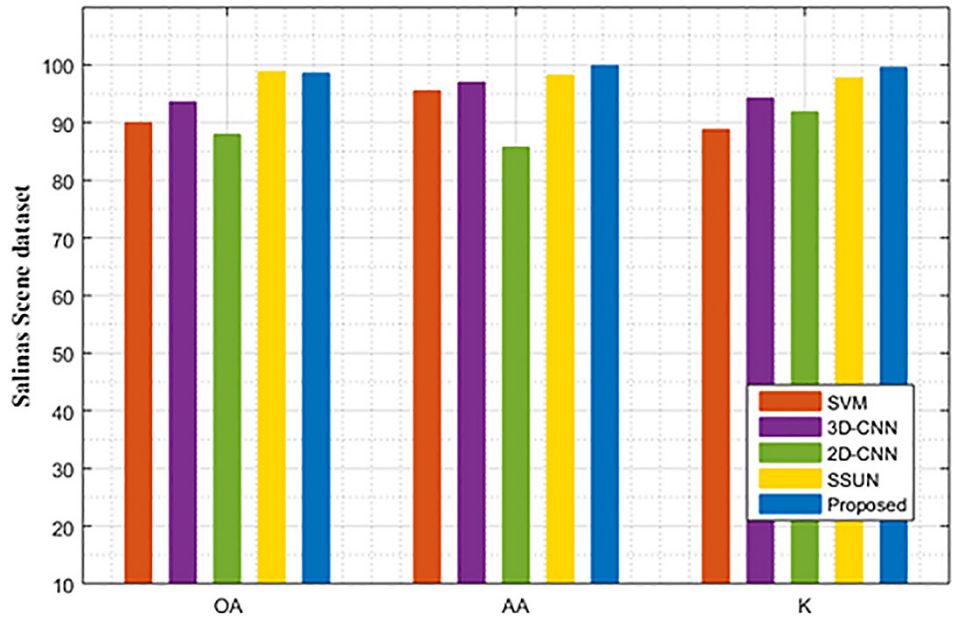

Figure 6. Classification comparison results on SS dataset.

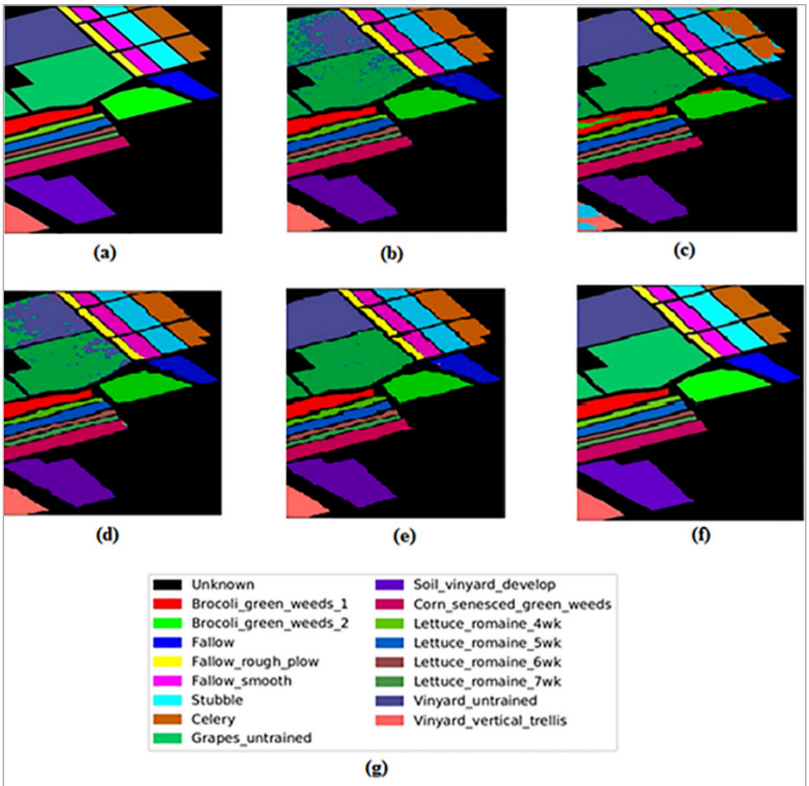

Figure 7. SS dataset classification map. (a) Ground truth, (b) 2D-CNN, (c) SVM, (d) SSUN, (e) 3D-CNN, (f) proposed and (g) legend.

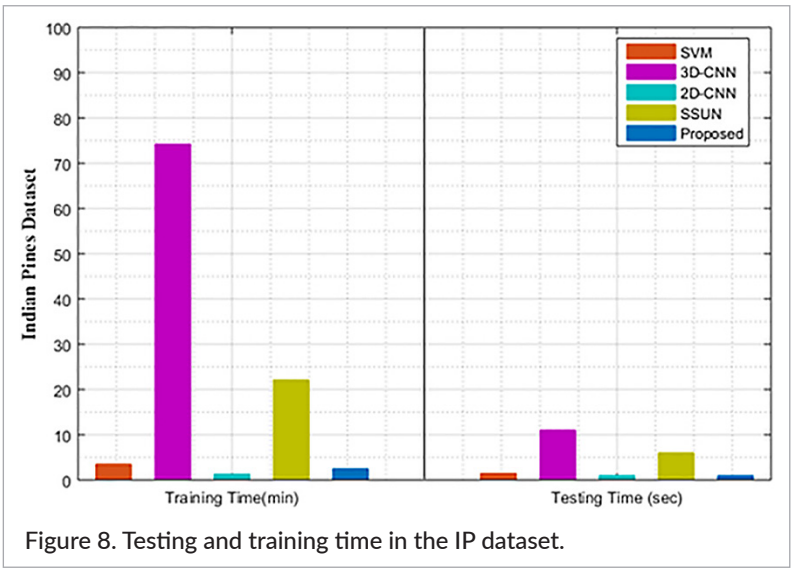

Figure 8. Testing and training time in the IP dataset.

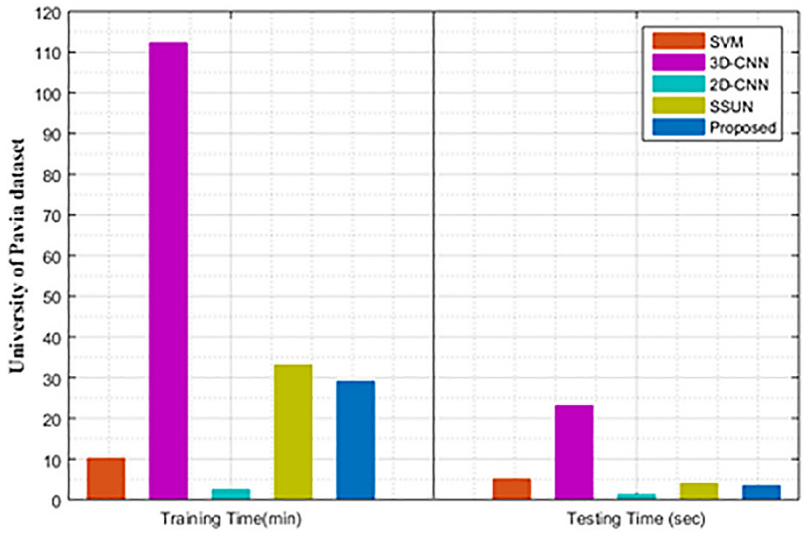

Figure 9. Testing and training time in the PU dataset.

parameter value results in reaching the highest classification accuracy.

In terms of factors for evaluating classification and computational time, the designed architecture outperforms all existing strategies, and its classification map is compared with the ground truth with high classification accuracy.

In addition, when compared to other spectro–spatial classification methods, the proposed method has improved performance and provides very satisfactory classification, according to the comparative analysis. As a result, it is possible to preserve spatial and spectral information while reducing the size of hyperspectral data to improve classification accuracy. Also, the proposed cycle-GAN is not supreme in aspects of computation time, the time of processing is still competitive with several other methods of classification.

Conclusion

Many applications rely on the classification of remote sensing images. These include natural disaster detection, coverage management and land resource utilisation. As a result, the cycle-GAN architecture classification is proposed. Three benchmark datasets are used to compare experimental results to state-of-the-art methods. The proposed architecture focuses on hyperspectral images classification from remote sensing images. The OA, AA and Kappa coefficients have all increased by varying

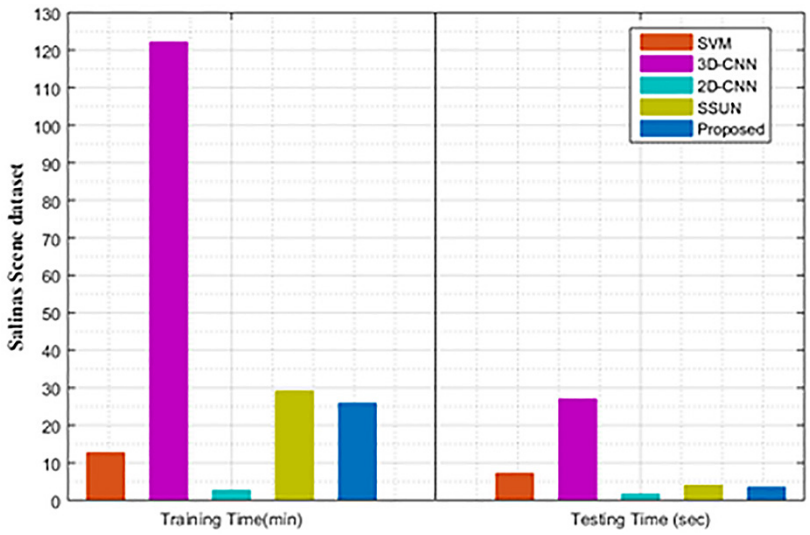

Figure 10. Testing and training time in SS dataset.

Table 5. Testing (s) and training (min) for IP, PU and SS datasets for various HSI classification techniques.

Methods	IP		PU		SS	
	Training duration	Testing duration	Training duration	Testing duration	Training duration	Testing duration
SVM	3.5	1.5	10.2	5.1	12.7	7.2
3D-CNN	74.24	11	112.32	23.12	122.15	27
2D-CNN	1.27	1	2.5	1.3	2.7	1.7
SSUN	22.1	6	33.12	4	29.12	4
Proposed method cycle-GAN	20.5	5.1	29.12	3.5	25.9	3.5

degrees in the SS, IP and PU datasets. Furthermore, the cycle-GAN is not the best in terms of processing speed, and its computation time is still competitive with many other classification methods. It is considered to improve the network structure in the future. In this study, the proposed method also generates images without using labels, and its categories are unknown. As a result, each category's ability to extract features has improved uniformly.

References

1. A. Qin, Z. Shang, J. Tian, Y. Wang, T. Zhang and Y.Y. Tang, "Spectral–spatial graph convolutional networks for semisupervised hyperspectral image classification", *IEEE Geosci. Remote Sens. Lett.* **16(2),** 241–245 (2019). https://doi.org/10.1109/LGRS.2018.2869563
2. S. Zhou, Z. Xue and P. Du, "Semisupervised stacked autoencoder with cotraining for hyperspectral image classification", *IEEE Trans. Geosci. Remote Sens.* **57(6),** 3813–3826 (2019). https://doi.org/10.1109/TGRS.2018.2888485
3. C. Liu, J. Li and L. He, "Superpixel-based semisupervised active learning for hyperspectral image classification", *IEEE J. Select. Topics Appl. Earth Observ. Remote Sens.* **12(1),** 357–370 (2019). https://doi.org/10.1109/JSTARS.2018.2880562
4. L. Mou, X. Lu, X. Li and X.X. Zhu, "Nonlocal graph convolutional networks for hyperspectral image classification", *IEEE Trans. Geosci. Remote Sens.* **58(12),** 8246–8257 (2020). https://doi.org/10.1109/TGRS.2020.2973363
5. Z. Zhang, "Semi-supervised hyperspectral image classification algorithm based on graph embedding and discriminative spatial information", *Microproc. Microsyst.* **75,** 103070 (2020). https://doi.org/10.1016/j.micpro.2020.103070
6. Y. Hu, R. An, B. Wang, F. Xing and F. Ju, "Shape adaptive neighborhood information-based semi-supervised learning for hyperspectral image classification", *Remote Sens.* **12(18),** 2976 (2020). https://doi.org/10.3390/rs12182976
7. Y. Zhao, F. Su and F. Yan, "Novel semi-supervised hyperspectral image classification based on a superpixel graph and discrete potential method", *Remote Sens.* **12(9),** 1528 (2020). https://doi.org/10.3390/rs12091528
8. Y. Zhang, G. Cao, X. Li, B. Wang and P. Fu, "Active semi-supervised random forest for hyperspectral image classification", *Remote Sens.* **11(24),** 2974 (2019). https://doi.org/10.3390/rs11242974
9. Z. Xue, "Semi-supervised convolutional generative adversarial network for hyperspectral image classification", *IET Image Proc.* **14(4),** 709–719 (2020). https://doi.org/10.1049/iet-ipr.2019.0869
10. W. Zhao, X. Chen, Y. Bo and J. Chen, "Semisupervised hyperspectral image classification with cluster-based conditional generative adversarial net", *IEEE Geosci. Remote Sens. Lett.* **17(3),** 539–543 (2019). https://doi.org/10.1109/LGRS.2019.2924059
11. X. Ji, Y. Cui, H. Wang, L. Teng, L. Wang and L. Wang, "Semisupervised hyperspectral image classification using spatial-spectral information and landscape features", *IEEE Access* **7,** 146675–146692 (2019). https://doi.org/10.1109/ACCESS.2019.2946220
12. Z. Zhong, J. Li, D.A. Clausi and A. Wong, "Generative adversarial networks and conditional random fields for hyperspectral image classification",

IEEE Trans Cybernet. **50(7),** 3318–3329 (2019). https://doi.org/10.1109/TCYB.2019.2915094

13. A. Sellami, M. Farah, I.R. Farah and B. Solaiman, "Hyperspectral imagery classification based on semi-supervised 3-D deep neural network and adaptive band selection", *Expert Syst. Applic.* **129,** 246–259 (2019). https://doi.org/10.1016/j.eswa.2019.04.006
14. S. Ren, S. Wan, X. Gu, P. Yuan and H. Xu, "Semi-supervised hyperspectral image classification using local low-rank representation", *Remote Sens. Lett.* **10(2),** 195–204 (2019). https://doi.org/10.1080/2150704X.2018.1538581
15. L. Mou, X. Lu, X. Li and X.X. Zhu, "Nonlocal graph convolutional networks for hyperspectral image classification", *IEEE Trans. Geosci. Remote Sens.* **58(12),** 8246–8257 (2020). https://doi.org/10.1109/TGRS.2020.2973363
16. K. Gao, B. Liu, X. Yu, J. Qin, P. Zhang and X. Tan, "Deep relation network for hyperspectral image few-shot classification", *Remote Sens.* **12(6),** 923 (2020). https://doi.org/10.3390/rs12060923
17. S. Huang, H. Zhang, and A. Pižurica, "Semisupervised sparse subspace clustering method with a joint sparsity constraint for hyperspectral remote sensing images", *IEEE J. Select. Topics Appl. Earth Observ. Remote Sens.* **12(3),** 989–999 (2019). https://doi.org/10.1109/JSTARS.2019.2895508
18. A. Sellami, A.B. Abbes, V. Barra and I.R. Farah, "Fused 3-D spectral-spatial deep neural networks and spectral clustering for hyperspectral image classification", *Pattern Recogn. Lett.* **138,** 594–600 (2020). https://doi.org/10.1016/j.patrec.2020.08.020
19. J. Xia, W. Liao and P. Du, "Hyperspectral and Lidar classification with semisupervised graph fusion", *IEEE Geosci. Remote Sens. Lett.* **17(4),** 666–670 (2019). https://doi.org/10.1109/LGRS.2019.2928009
20. J. Xu, G. Feng, T. Zhao, X. Sun and M. Zhu, "Remote sensing image classification based on semi-supervised adaptive interval type-2 fuzzy c-means algorithm", *Comput. Geosci.* **131,** 132–143 (2019). https://doi.org/10.1016/j.cageo.2019.06.005
21. Y. Wu, G. Mu, C. Qin, Q. Miao, W. Ma and X. Zhang, "Semi-supervised hyperspectral image classification via spatial-regulated self-training", *Remote Sens.* **12(1),** 159 (2020). https://doi.org/10.3390/rs12010159
22. B. Cui, X. Xie, S. Hao, J. Cui and Y. Lu, "Semi-supervised classification of hyperspectral images based on extended label propagation and rolling guidance filtering", *Remote Sens.* **10(4),** 515 (2018). https://doi.org/10.3390/rs10040515
23. Y. Zhao, F. Su and F. Yan, "Novel semi-supervised hyperspectral image classification based on a superpixel graph and discrete potential method", *Remote Sens.* **12(9),** 1528 (2020). https://doi.org/10.3390/rs12091528
24. L.P.K. Boggavarapu and P. Manoharan, "A new framework for hyperspectral image classification using Gabor embedded patch based convolution neural network", *Infrared Phys. Technol.* **110,** 103455 (2020). https://doi.org/10.1016/j.infrared.2020.103455
25. F. Xie, Q. Gao, C. Jin and F. Zhao, "Hyperspectral image classification based on superpixel pooling convolutional neural network with transfer learning", *Remote Sens.* **13(5),** 930 (2021). https://doi.org/10.3390/rs13050930
26. M. Ramamurthy, Y.H. Robinson, S. Vimal and A. Suresh, "Auto encoder based dimensionality reduction and classification using convolutional neural networks for hyperspectral images", *Microproc. Microsyst.* **79,** 103280 (2020). https://doi.org/10.1016/j.micpro.2020.103280
27. A. Mohan and M. Venkatesan, "HybridCNN based hyperspectral image classification using multiscale spatiospectral features", *Infrared Phys. Technol.* **108,** 103326 (2020). https://doi.org/10.1016/j.infrared.2020.103326